

1 **Response to Anonymous Referee #3 follow-up comments**
2

3 Follow-up Reviewer Comment: Results presented by the authors in Table 1 suggest that the
4 supermicron-diameter aerosol size fractions were acidic, which is consistent with expectations based on
5 kinetics. Alkalinity associated with freshly produced particles is typically titrated within seconds to a few
6 minutes by multiple pathways of which condensation and subsequent in situ oxidation of SO₂ in only
7 one. Condensation of acids from the gas phase (including HNO₃, HCl, H₂SO₄, HCOOH, and CH₃COOH
8 among others) also titrates alkalinity associated with, and thereby acidifies, freshly produced crustal
9 dust as well as marine aerosol. Following alkalinity titration, pH drops sharply and the SO₂ pathway
10 becomes insignificant [e.g., Chameides and Stelson, 1992, JGR]. Measurements in many regions
11 demonstrates that H₂SO₄ is generally not the primary source of acidity in supermicron-diameter aerosol
12 size fractions. The authors present no evidence to support the speculation that the in situ oxidation of
13 SO₂ is the only or even most important process by which larger particles are acidified. I encourage them
14 to drop the unsubstantiated suggestion that the in situ oxidation of SO₂ is the only driver of acidification.
15 The primary point in this section of the manuscript relates to aerosol pH and associated bioavailability of
16 Fe, not to the processes by which aerosols are acidified.

17
18 **Response:** *We are merely quoting the conclusions of Meskhidze et al. (2003) here and further discussion is
19 not merited. In response to the concerns the statement now reads "...and the subsequent acidification of
20 dust through heterogeneous and gas phase processes, Meskhidze et al. (2003) concluded that..."*

21
22 Follow-up Reviewer Comment: pH is a mathematical expression of H⁺ concentration, which has physical
23 meaning that does not change based on the application. Direct averages of pH values yield H⁺
24 concentrations that are biased relative to average H⁺ concentrations expressed as pH. It is evident that
25 direct averages of pH values have no physical meaning. It appears that the authors' wish to report a
26 population statistic for the central tendency of the distribution of solution acidities rather than the
27 average for that distribution of solution acidities. As such, I suggest that they report the median pH,
28 which does have physical meaning. Other properties of the aerosol are reported in the paper as average
29 concentrations (e.g., Fig. 4). The pH value corresponding to the average H⁺ concentration is the only
30 unbiased statistic relevant for direct comparison to and interpretation in the context of averages for
31 other aerosol properties.

32
33 **Response:** *We understand the concerns but these are minor issues because i) Both medians and averages
34 were reported since the first version of the paper, and, ii) they differ at most by 0.11 pH units.*

35
36 Follow-up Reviewer Comment: NSS K⁺ has virtually no direct effect on solution pH. For example, adding
37 NSS K⁺ to an aerosol solution in the form of KBr or K₂SO₄ and at a concentration relevant to particles
38 from biomass burning would have essentially no influence on either the actual or the calculated acidity
39 of that solution. In contrast to the authors' suggestion in the manuscript, simple correlations between
40 NSS K⁺ and acidity in aerosols produced by biomass burning do not demonstrate a significant causal
41 influence of NSS K⁺ in "rendering aerosol more alkaline." To suggest otherwise is misleading. The text
42 should be clarified. In addition, since all pHs reported in the manuscript correspond to acidic solutions,
43 it would seem more appropriate to characterize biomass-burning impacted aerosol as "less acidic" rather
44 than "more alkaline."

45
46 **Response:** *According to Figure S5, slight shifts in pH (which could be from including NSS-K in the
47 calculations) when it is around 3 can lead to a strong response in nitrate. By definition "less acidic" means
48 "more alkaline", but we will make the suggested change and the sentence will now read "...could possibly
49 be associated with higher concentrations of NSS-K (Zhang et al. 2015), rendering aerosol less acidic".*

50

51

52

53 **Particle water and pH in the Eastern Mediterranean: Sources variability and**
54 **implications for nutrients availability.**

55
56 P. Nikolaou[#]=A. Bougiatioti^{1,2,*}, P. Nikolaou¹, I. Stavroulas¹, G. Kouvarakis¹, R. Weber², A.
57 Nenes^{2,3,4}, M. Kanakidou¹, and N. Mihalopoulos^{1,4,*}

58
59 1 Environmental Chemical Processes Laboratory, University of Crete, 71003 Crete, Greece
60 2 School of Earth and Atmospheric Sciences, Georgia Institute of Technology, Atlanta, GA 30332, USA
61 3 School of Chemical and Biomolecular Engineering, Georgia Institute of Technology, Atlanta, GA, 30332,
62 USA
63 4 IERSD, National Observatory of Athens, Athens, GR-15236, Greece.

64
65 Keywords: aerosols, water content, pH, availability, nutrients
66
67 (*) Correspondence to: mihalo@uoc.gr ; kbougiatioti@gmail.com
68

69 **Abstract**
70 Particle water (LWC) and aerosol pH are important parameters of the aerosol phase, affecting
71 heterogeneous chemistry and bioavailability of nutrients that profoundly impact cloud formation,
72 atmospheric composition and atmospheric fluxes of nutrients to ecosystems. Few measurements
73 of in-situ LWC and pH however exist in the published literature. Using concurrent measurements
74 of aerosol chemical composition, cloud condensation nuclei activity and tandem light scattering
75 coefficients, the particle water mass concentrations associated with the aerosol inorganic (W_{inorg})
76 and organic (W_{org}) components are determined for measurements conducted at the Finokalia
77 atmospheric observation station in the eastern Mediterranean between August and November
78 2012. These data are interpreted using the ISORROPIA-II thermodynamic model to predict pH of
79 aerosols originating from the various sources that influence air quality in the region. On average,
80 closure between predicted aerosol water and that determined by comparison of ambient with dry
81 light scattering coefficients was achieved to within 8% (slope=0.92, $R^2=0.8$, n=5201 points).
82 Based on the scattering measurements a parameterization is also derived, capable of reproducing

83 the hygroscopic growth factor ($f(RH)$) within 15% of the measured values. The highest aerosol
84 water concentrations are observed during nighttime, when relative humidity is highest and the
85 collapse of the boundary layer increases the aerosol concentration. A significant diurnal variability
86 is found for W_{org} with morning and afternoon average mass concentrations being 10-15 times lower
87 than nighttime concentrations, thus rendering W_{inorg} the main form of particle water during
88 daytime. The average value of total aerosol water was $2.19 \pm 1.75 \mu\text{g m}^{-3}$, contributing on average
89 up to 33% of the total submicron mass concentration. Average aerosol water associated with
90 organics, W_{org} , was equal to $0.56 \pm 0.37 \mu\text{g m}^{-3}$, thus organics contributed about 27.5% to the total
91 aerosol water, mostly during early morning, late evening and nighttime hours.

92 The aerosol was found to be highly acidic with calculated aerosol pH varying from 0.5 to 2.8
93 throughout the study period. Biomass burning aerosol presented the highest values of pH in the
94 submicron fraction and the lowest values in total water mass concentration. The low pH values
95 observed in the submicron mode and independently of air masses origin could increase nutrient
96 availability and especially P solubility, which is the nutrient limiting sea water productivity of the
97 eastern Mediterranean.

98

99 **1. Introduction**

100 Atmospheric particles have the ability to absorb significant amounts of water, which profoundly
101 affects their physical and chemical properties (Khlystov et al., 2005), and impacts on atmospheric
102 processes and health. Ambient concentrations of aerosol liquid water are controlled by the aerosol
103 chemical composition, relative humidity (RH) and temperature, as it is largely in chemical
104 equilibrium with the surrounding water vapor. Liquid water is ubiquitous and exceeds the total
105 aerosol dry mass by 2 to 3 times on a global scale (Liao and Seinfeld, 2005). Therefore, the aerosol
106 liquid water content (LWC) increases the particle size, affecting the particle lifetime and scattering
107 efficiency. LWC and its strong dependence on relative humidity (RH) are the most important
108 contributors to aerosol direct radiative cooling by aerosols (Pilinis et al., 1995). Numerous
109 modeling studies suggest that reactions in aerosol liquid water are an important pathway of
110 secondary organic aerosol (SOA) formation (Carlton and Turpin, 2013; Myriokefalitakis et al.,
111 2011), thus playing an important role in the overall aerosol chemical composition. Aerosol water
112 also has profound impact on the aerosol phase state, being able to transform semi-solid and viscous

114 particles into homogeneous phase that are in equilibrium with their environment (Pöschl and
115 Shiraiwa, 2015). This affects the timescale of heterogeneous reactions and ice nucleation.
116 Nevertheless, despite the abundance and importance of LWC, it is not routinely measured, actual
117 mass concentrations are uncertain, especially in the presence of organic compounds and model
118 predictions of the property are often not evaluated (Nguyen et al., 2014).

119 Apart from the LWC, the pH of aqueous aerosols is another critically important aerosol property
120 that drives many processes related to the aerosol chemical composition and gas-aerosol
121 partitioning (Guo et al., 2015; Surratt et al., 2007; 2010; Meskhidze et al., 2003; Eddingsaas et al.,
122 2010; Myriokefalitakis et al., 2015). Direct measurements of aerosol pH “*in situ*” are scarce (e.g.,
123 Keene et al., 2002; 2004) and require careful considerations owing to the non-conserved nature of
124 the hydronium ion and partial dissociation of inorganic and organic electrolytes in the aerosol.
125 These challenges have led to the suggestion that indirect alternatives – such as measuring the semi-
126 volatile partitioning of key species sensitive to pH, combined with comprehensive models may
127 provide a reasonably accurate estimate of pH that can be carried out with routine measurements
128 (Hennigan et al., 2015). The most frequently used proxy is the “ion balance”, where the charge
129 balance of measurable anions and cations is calculated, with the exception of the hydronium and
130 hydroxyl ions; a surplus of cations implies an alkaline aerosol and vice versa. Often it is implied
131 that a larger value of the ion balance implies a stronger acidity/alkalinity. As shown by Hennigan
132 et al. (2015) and Guo et al. (2015), the ion balance (and other similar proxies discussed in Hennigan
133 et al., 2015) fail in general to represent the true aerosol pH; only meticulous measurement of semi-
134 volatile species (such as ammonia/ammonium) and other aerosol chemical constituents, combined
135 with appropriate thermodynamic calculations (e.g. with ISORROPIA-II; Fountoukis and Nenes,
136 2007) are able to realistically provide particle pH and LWC (Hennigan et al., 2015). For an
137 accurate and unbiased pH calculation both gas and aerosol phase concentrations are needed,
138 however, when some uncertainty can be tolerated or the level of pH bias is known, aerosol
139 measurements alone can still be quite informative for determining the pH, as demonstrated by Guo
140 et al. (2015).

141 Directly linked to aerosol pH and LWC is the bioavailability of nutrients contained within dust,
142 involving pH-dependent catalyzed redox-reaction pathways; upon deposition, increased
143 availability of these nutrients may promote primary productivity in continental and marine
144 ecosystems (e.g., Meskhidze et al., 2003; Nenes et al., 2011; Mahowald et al., 2008; 2009;

145 Krishnamurthy et al., 2010). Acids (such as sulfuric and nitric) generated in the atmosphere from
146 a variety of anthropogenic and biogenic sources, when mixed with mineral aerosols in sufficient
147 amounts could lower the aerosol pH to values that increase the solubilities of Fe and P-containing
148 minerals by several orders of magnitude (Stumm and Morgan, 1996; Shi et al., 2012). Nenes et al.
149 (2011) have demonstrated that acidification can release considerable amounts of soluble
150 phosphorus from soil-laden minerals (e.g., 81-96% of the total P found in Saharan dust and soil).
151 Apart from P, the transport and deposition of mineral dust is believed to be a major, if not the
152 dominant source of Fe to the remote ocean (Jickells et al., 2005). Considering the mixing of SO₂
153 with advected dust plumes and the subsequent acidification of dust through heterogeneous and gas
154 phase processes, through heterogeneous oxidation of the SO₂ on deliquescent dust particles within
155 the plume, Meskhidze et al. (2003) concluded that for aerosol with pH <2, 1-2% of the contained
156 Fe would be mobilized within 3-5 days. Meskhidze et al., (2005) also demonstrated that sufficient
157 acidification of Asian dust plumes could drive, upon deposition, a phytoplankton bloom in High
158 Nitrate Low Chlorophyll regions of the North Atlantic. Solmon et al. (2009) also showed that
159 simulated enhancements in particulate soluble iron driven by the chemical dissolution mechanism,
160 can range from 0.5 to 6%, which is consistent with observations over the North Pacific Ocean.
161 The Eastern Mediterranean, being at the nexus of three continents (Europe, Asia and Africa),
162 receives air masses influenced by a spectrum of human (traffic, biomass burning and industry) and
163 natural (dust and marine) sources. It is therefore an ideal location to study atmospheric
164 acidification of aerosols; very few studies however to date have accomplished that.
165 This study uses aerosol chemical composition measurements in conjunction with cloud
166 condensation nuclei (CCN) concentration and light scattering coefficient (σ_{sp}) measurements to
167 model the water mass concentrations (LWC) of aerosols from various sources in the Eastern
168 Mediterranean. These data are then used in combination with the ISORROPIA-II thermodynamic
169 equilibrium model (Fountoukis and Nenes, 2007) to predict the aerosol pH for air masses that
170 influenced air quality in the Eastern Mediterranean during the late summer and fall months of
171 2012.
172

173 **2. Instrumentation and Methods**

174 **2.1 Measurement site**

175 Aerosol measurements were conducted at the Finokalia atmospheric observation station in Crete,
176 Greece (35°20'N, 25°40'E, 250m a.s.l.) between August and November 2012. The site
177 (<http://finokalia.chemistry.uoc.gr/>) is a European supersite for atmospheric aerosol research and is
178 part of the ACTRIS Network (Aerosols, Clouds, and Trace gases Research Infrastructure)
179 (<http://www.actris.eu/>). The station is located at the northeastern part of the island of Crete, facing
180 the Mediterranean Sea covering the whole northern sector. Being away from direct urban
181 influence, the station is representative for background measurements in the Eastern Mediterranean
182 and sampled air masses arriving at the site have most commonly a marine source region or
183 originate from continental Europe and Greek mainland. Moreover, dust events from Northern
184 Africa (Sahara) occur often during spring and autumn. More details for the Finokalia station and
185 the prevailing climatology in the area are given by Mihalopoulos et al. (1997).

186

187 **2.2 Instrumentation**

188 PM₁ (Particulate Matter of diameter smaller than 1 μm) aerosol light scattering coefficients (σ_{sp})
189 were measured online with the use of two different nephelometers to infer the LWC. Particle dry
190 scattering was measured with a 3-wavelength Aurora 1000 Integrating Nephelometer, located in
191 an air-conditioned sampling trailer and operated with a diffusional silica dryer upstream, which
192 maintained the RH below 35%. Based on the ISORROPIA model run for metastable ammonium sulfate
193 aerosol at an RH of 30%, the maximum water which can be contained under these conditions is 1.21 $\mu\text{g m}^{-3}$,
194 which is less than 12% of the total submicron aerosol mass. The nephelometer for the particle wet
195 scattering was a Radiance Research M903, located outside the trailer in order to provide a
196 scattering measurement at ambient T and RH. This second nephelometer was equipped with a
197 VAISALA Inc. Humitter 50U Integrated Humidity and Temperature probe in order to record the
198 ambient values of T and RH with an accuracy at 20 °C specified to be better than $\pm 5\%$ RH. Both
199 nephelometers take part in yearly intercomparisons within the ACTRIS network.

200 The real-time, quantitative measurements of the non-refractory components of the submicron
201 aerosol were provided by an Aerosol Research Inc. Aerosol Chemical Speciation Monitor (ACSM;
202 Ng et al., 2011). Ambient air was draw into the ACSM by a multiple PM₁₀ (Particulate Matter of
203 diameter smaller than 10 μm) aerosol inlet operating at Finokalia, with a temporal resolution of 30

204 minutes. At the inlet of the ACSM and via a critical aperture mounted at the entrance of an
205 aerodynamic lens, the submicron fraction of the aerosol is sampled. The aerodynamic lens of the
206 ACSM allows for the detection of particles up to 700 nm diameter. The focused particle beam is
207 then transmitted through two vacuum chambers and into a detection chamber where the particles
208 impact on a hot plate and flash vaporized. Finally they are detected and characterized with the use
209 of an electron impact quadrupole mass spectrometer. Constituents quantified by the ACSM include
210 organics, sulfate, ammonium, nitrate and chloride. Detection limits for all constituents for 30 min
211 of averaging time are provided by Ng et al. (2011) and are for ammonium, organics, sulfate, nitrate,
212 and chloride are $0.284 \mu\text{g m}^{-3}$, $0.148 \mu\text{g m}^{-3}$, $0.024 \mu\text{g m}^{-3}$, $0.012 \mu\text{g m}^{-3}$, and $0.011 \mu\text{g m}^{-3}$,
213 respectively. Mass concentrations are calculated with the recommended collection efficiency of
214 0.5 for all constituents (Ng et al. 2011) and the main aerosol constituents i.e. organics, sulfate and
215 ammonium are verified by comparison with other concurrent measurements (daily PM₁ filters;
216 Bougiatioti et al. (2014) supplementary material). PM₁ filters (Pallflex Tissuquartz, 47 mm
217 diameter) were collected using a built-in system comprised of the four upper stages (stage 8-11)
218 of a low-pressure Berner impactor (PLBI; Berner and Lürzer, 1980). Furthermore, daily PM₁₀
219 filters are also collected on site using a sequential sampler (Leckel, SEQ47/50). A detailed study
220 of the comparison between ACSM and PM₁ filter values for a large subset of the present data
221 (16/08-30/09/2012) is provided by Bougiatioti et al. (2014).

222 PM₁ and PM₁₀ filters were analyzed by ion chromatography (IC) for anions (Cl⁻, Br⁻, NO₃⁻
223 (nitrate), SO₄⁻² (sulfate), C₂O₄⁻² (oxalate)) and cations (K⁺, Na⁺, NH₄⁺, Mg²⁺, Ca²⁺) using the
224 procedure described by Bardouki et al. (2003). From the calcium, the crustal component can be
225 estimated by subtracting the contribution of sea-salt Ca²⁺ = [Na]^{*}0.038 and dust concentration is
226 estimated using the approach of Sciare et al. (2005). Based on the study by Koulouri et al. (2008)
227 for a two-year period at the same sampling site, it has been demonstrated that for fine particles (in
228 that case D_a<1.3 μm) the contribution of the marine source to the aerosol mass was 10%. Similarly,
229 dust contribution in the fine fraction can vary between 6 and 10% for summer and winter,
230 respectively.

231 From 25/6 to 7/8/2014, gas phase ammonia measurements were also conducted at Finokalia, using
232 a wet annular denuder (WAD; Wyers et al., 1993; Spindler et al., 2003) coupled with an ion
233 chromatography system quantifying cations with an hourly resolution in order to check the validity
234 of our calculations in the absence of gaseous phase NH₃ (see section 2.4). Concurrent black carbon

235 (BC) measurements were performed on site using a seven-wavelength aethalometer (Magee
236 Scientific, AE31) with a time resolution of 5 min. Based on previous studies at Finokalia, BC is
237 found mainly on the fine aerosol fraction (Koulouri et al., 2008; Bougiatioti et al., 2014) hence
238 these values are used in addition to the ACSM concentrations to calculate the dry aerosol mass of
239 the PM₁ fraction.

240 Size-selected cloud condensation nuclei (CCN) measurements were obtained using a Droplet
241 Measurement Technologies, Continuous Flow Streamwise Thermal Gradient CCN counter
242 (CFSTGC). Particles of 60, 80, 100 and 120 nm were first size-selected by a differential mobility
243 analyzer (DMA), split into two and one of these flows was introduced in the CCN counter. The
244 total number of condensation nuclei (CN) was measured by a condensation particle counter (CPC;
245 TSI 1772) situated downstream the first DMA. In the CCN counter, the activated droplets are sized
246 and counted by an optical particle counter (OPC) after exiting the growth chamber. The instrument
247 was operated in scanning flow CCN analysis mode (SFCA; Moore and Nenes, 2009), where the
248 flow rate in the growth chamber changes over time, while a constant temperature difference is
249 maintained. In that way the supersaturation changes continuously, providing activation spectra
250 with a high temporal resolution. The flow rate was increased linearly between a minimum and a
251 maximum flow rate and sigmoidal activation curves of CCN vs flow rate were recorded, with the
252 inflection point of the sigmoid representing a critical activation flow, Q_{50} , that corresponds to a
253 critical supersaturation, S^* , above which particles act as CCN. From the critical supersaturation
254 and knowledge of the particle dry diameter, with the application of Köhler theory, the
255 hygroscopicity parameter kappa (Petters and Kreidenweis, 2007) is obtained, which is then used
256 to determine the LWC associated with organic components of the aerosol (Guo et al., 2015).
257 Finally, analysis of 5-day back trajectories of air masses arriving at Finokalia at 1000 and 3000 m
258 above ground level every 6 h was conducted with the help of the HYSPLIT model
259 ([www.arl.noaa.gov /hysplit.php](http://www.arl.noaa.gov/hysplit.php); Stein et al., 2015).

260

261 **2.3 Determination of LWC from nephelometers**

262 The particle water was inferred using the approach of Guo et al. (2015), where the ratio of the wet
263 and dry PM₁ scattering coefficients (σ_{sp}) measured by the two nephelometers is used. For this, the
264 aerosol hygroscopic growth factor ($f(RH)$) is calculated according to a well-established method
265 based on the two scattering coefficients: $f(RH) = \sigma_{sp(wet)} / \sigma_{sp(dry)}$ (e.g. Sheridan, 2002; Magi, 2003;

266 Kim et al., 2006). These scattering coefficients in ambient and dry conditions are proportional to
 267 the diameter of average surface $\overline{D_p}$ and the average scattering coefficients $\overline{Q_s}$, so that :

$$268 \quad \overline{D_{p,ambient}} = \overline{D_{p,dry}} \sqrt{f(RH) \overline{Q_{s,dry}} / \overline{Q_{s,ambient}}} \quad (1)$$

269 Assuming that the two average scattering efficiencies are almost equal, LWC is then equal to the
 270 difference between ambient and dry particle volume, and by substitution of the dry diameter of
 271 average surface:

$$272 \quad \overline{D_{p,dry}}^3 = \frac{m_p}{\left(\frac{\pi}{6}\right) \rho_p N_t} \quad (2)$$

273 where N_t is the total number concentration, ρ_p is the density of dry aerosol and m_p is the dry mass
 274 concentration, we arrive at the simplified expression of:

$$275 \quad LWC = [f(RH)^{1.5} - 1] \frac{m}{\rho_p} \quad (3)$$

276 The simplification assumption that the dry and ambient scattering efficiencies are almost equal
 277 introduces an error in the derived LWC, which based on the detailed analysis of Guo et al. (2015)
 278 is of the order of 10% at RH=76.4%, but can reach up to 21% at RH=90%.

279 For this set of measurements the PM₁ dry mass concentration is calculated from the sum of the
 280 ACSM constituents combined with the BC measurements. During the sampling period, the
 281 comparison between the sum of ACSM and BC masses and the submicron mass derived from a scanning
 282 mobility particle sizer (SMPS; TROPOS-type) is very good ($y=0.96x$, $R^2=0.67$ for a period of 2-years;
 283 Figure S3). Therefore the bias introduced by ignoring other refractory constituents than BC is minimal,
 284 which is in agreement with size-segregated aerosol chemical composition measurements already conducted
 285 at Finokalia (e.g. Koulouri et al., 2008). The particle density, ρ_p , was estimated from the particle
 286 composition from the ACSM ammonium, organics and sulfate, using an organic density of 1.35 g
 287 cm⁻³ as determined by Lee et al. (2010) for the same site during the summer of 2008, the density
 288 of ammonium sulfate (1.77 g cm⁻³) and the equation:

$$289 \quad \rho_p = \left[\frac{x_{a/s}}{\rho_{a/s}} + \frac{x_{org}}{\rho_{org}} \right]^{-1} \quad (4)$$

290 where $x_{a/s}$ is the mass fraction of ammonium sulfate and x_{org} is the mass fraction of the organics,
 291 and $\rho_{a/s}$ and ρ_{org} are the densities of ammonium sulfate and the organics, respectively. It must be

292 noted that nitrate is not taken into account as its concentrations are very close to the limit of
293 detection of the ACSM for the PM₁ fraction at the Finokalia site during the studied period. Particle
294 density was calculated to be $1.56 \pm 0.08 \text{ g cm}^{-3}$ (n=6028), with aerosol concentration ranging from
295 1.33 to $16.65 \text{ } \mu\text{g m}^{-3}$ and average value of $5.62 \pm 3 \text{ } \mu\text{g m}^{-3}$. The particle water calculated by this
296 method is hereafter referred to as $f(RH)_{\text{water}}$, with the uncertainty of this calculation being
297 estimated to be 23% (Guo et al., 2015).

298

299 **2.4 LWC and pH prediction from chemical composition**

300 The water vapor uptake by aerosol establishing equilibrium for ambient temperature and relative
301 humidity conditions is influenced by both inorganic and organic components. LWC, therefore, is
302 directly dependent on aerosol chemical composition and meteorological conditions, as well. As
303 proposed by Guo et al. (2015) and explained below, we calculated the particle water associated
304 with inorganics (W_{inorg}) and the particle water associated with organics (W_{org}). The sum of these
305 two ($W_{\text{inorg}} + W_{\text{org}}$), equal to the total particle water, is then compared to the LWC determined by
306 the two nephelometers.

307 First the particle pH was calculated by the thermodynamic model ISORROPIA-II for the PM₁
308 aerosol fraction. W_{inorg} was calculated based on a thermodynamic equilibrium between an
309 inorganic aerosol (NH₄-SO₄-NO₃-Cl-Na-Ca-K-Mg-water) and its gas phase precursors. For the
310 current analysis, the inputs to ISORROPIA-II are the inorganic ions measured by the ACSM with
311 a 30 min time resolution (except for Cl which is at the detection limit of the instrument at the
312 specific site), the average daily values for Na⁺, Cl⁻, Ca²⁺, K⁺ and Mg²⁺ determined by ion
313 chromatography analysis of PM₁ filters, and RH and T measured by the ambient nephelometer
314 probe. The use of daily values for the macromineral elements obtained from the filter analysis
315 could introduce potential artifacts in the calculation, but is believed to be limited as almost 90%
316 of the fine fraction mass in the area can be attributed to ammonium sulfate and organics (Koulouri
317 et al., 2008; Bougiatioti et al., 2009;2013).

318 The contribution of the organic components to particle water (W_{org}) was determined from the
319 organic hygroscopicity parameter (κ_{org}) from the observed CCN activities of the organic fraction
320 (Cerully et al., 2014):

321

$$W_{org} = \frac{m_s}{\rho_s} \frac{\kappa_{org}}{\left(\frac{1}{RH} - 1 \right)} \quad (5)$$

322 where m_s and ρ_s are the organic mass concentration from the ACSM and an organic density,
 323 respectively determined as described in section 2.3.

324 Finally, the particle pH is calculated by the thermodynamic model ISORROPIA-II (Fountoukis
 325 and Nenes, 2007) based on the calculated equilibrium particle hydronium ion concentration in the
 326 aerosol. As ISORROPIA-II does not take into account the LWC associated with the organic
 327 aerosol, a recalculation of pH is made by considering the predicted particle hydronium ion
 328 concentration per volume of air (H^{+}_{air}) and the total predicted water ($W_{inorg} + W_{org}$) (Guo et al.,
 329 2015):

330

$$pH = -\log_{10} H^{+}_{aq} = -\log \frac{1000 H^{+}_{air}}{W_{inorg} + W_{org}} \quad (6)$$

331 where the modeled concentrations for LWC and H^{+}_{air} are $\mu\text{g m}^{-3}$, and H^{+}_{aq} (mol L^{-1}) is the
 332 hydronium concentration in an aqueous solution and W_{inorg} and W_{org} are in $\mu\text{g m}^{-3}$. ISORROPIA-
 333 II has been previously tested and was able to predict the equilibrium partitioning of ammonia and
 334 nitric acid to within measurement uncertainty (Nowak et al., 2006; Fountoukis et al., 2009;
 335 Hennigan et al., 2015; Guo et al., 2015). Here, ISORROPIA-II was run in the “forward mode”
 336 assuming a metastable aerosol state. It should be noted that gas phase measurements of ammonia
 337 ($\text{NH}_3(g)$) were generally not available for the whole measurement period and the sum of NH_3 and
 338 NH_4^+ is assumed to be equal to NH_4^+ . Therefore it is expected that the pH could be underpredicted
 339 by at most one unit (Guo et al., 2015; Weber et al., 2016).

340 To assess the uncertainty in our calculations by not including gas phase NH_3 , a sensitivity analysis
 341 is performed by adding different amounts of $\text{NH}_3(g)$ to the system and quantifying the response in
 342 pH. Initial results of ISORROPIA, were compared to results obtained after adding 0.5, 1.2, 3.2 and
 343 5 $\mu\text{g m}^{-3}$ of ammonia. The values of 1.2 and 3.2 $\mu\text{g m}^{-3}$ were the median and maximum values of
 344 the gas phase measurements conducted with the WAD during summer 2014, respectively. These
 345 values are also within the observed values reported by Guo et al. (2015). A 3-year study conducted
 346 at the Finokalia station (Kouvarakis et al., 2001) reported that $\text{NH}_3(g)$ concentrations during
 347 summertime have an average of 0.27 $\mu\text{g m}^{-3}$ (range from 0.07 to 0.68 $\mu\text{g m}^{-3}$). Thus, a lower value
 348 (0.5 $\mu\text{g m}^{-3}$) to represent these measurements was also applied and finally 5 $\mu\text{g m}^{-3}$ was selected

349 as an extreme value which is very close to the European critical level for NH₃, established to 8 µg
350 m⁻³ as an annual mean (Air Quality Guidelines for Europe, 2000). The results of the sensitivity study
351 are provided in detail in the supplementary material and clearly show that neglecting the gas phase NH₃ in
352 the calculations leads to an underestimate of around 0.5 units in the pH (from 1.38 to 1.85 median values)
353 for the NH₃ range reported for Finokalia.

354 The above results are further supported by the partitioning of nitric acid between the condensed
355 (NO₃⁻) and gas phase (HNO₃). Assuming ideal solutions for the average conditions during the
356 study period derived from ISORROPIA-II, it is calculated that little nitrate should be present in
357 the aerosol phase when pH is lower than 3 (Figure S5 Supplementary). Indeed, with an average
358 concentration of nitrates of 0.12±0.06 µg m⁻³ in the fine mode and the resulting partitioning
359 coefficient of less than 0.2, it is derived that the maximum value of pH that can be observed for
360 the current conditions is 2. This value is in total accordance with the upper limit of pH of 1.85 derived
361 from the formerly presented sensitivity analysis.

362 For days where NH_{3(g)} measurements exist (summer 2014), following the same methodology as
363 before, the measured concentrations of NH_{3(g)} and predictions by the model are in fairly good
364 agreement. Observed gas phase concentrations have an of 0.79±0.27 µg m⁻³ while predicted
365 concentrations have an average of 0.65±0.32 µg m⁻³. Additionally, we directly compared the pH
366 and LWC values derived from ISORROPIA in the forward mode when calculations were initiated
367 with total (NH₃+NH₄⁺) versus paired results (n=328) for the respective ones initiated with only
368 particulate phase NH₄⁺. The results show that for the specific periods, the addition of NH₃ in the
369 calculations has a minor effect to both pH (y=0.965x, R²=0.584) and LWC (y=1.055x, R²=0.993).
370
371

372 **3. Results and Discussion**

373 **3.1 PM₁ chemical composition and f(RH)_water**

374 For the measurement period, the average values for the main aerosol constituents were 1.85±0.94,
375 2.31±1.61, 0.81±0.58 and 0.52±0.22 µg m⁻³ for organics, sulfate, ammonium and BC, respectively.
376 In terms of contribution to the PM₁ mass concentration, the two most abundant components of the
377 submicron range were sulfate and organics, with mass fractions of 39.6 and 33.8% respectively,
378 followed by ammonium (14.8%), BC (9.3%) and nitrate (2.1%). Chloride has a negligible
379 contribution to the total submicron mass concentration. The time series of the main aerosol

380 constituents and their overall contribution, as measured by the ACSM, are portrayed in Figure 1.
381 Nevertheless, a fluctuation of 10-20% in sulfate and/or ammonium concentrations is not expected
382 to be reflected in a pH change, given the logarithmic scale of the property, which is consistent with
383 the findings of Weber et al. (2016) that pH has a weak sensitivity to a wide range of SO_4^{2-} and
384 NH_3 . This is further elaborated by the sensitivity analysis of gas phase ammonia, where the 5-fold
385 increase of added amount of NH_3 causes a unit change in pH, on average. More details about the
386 ACSM measurements and performance can be found in Stavroulas et al. (in preparation, 2016).
387 The chemical composition is expected to influence the water content of aerosol, as well. Mean RH
388 and T during the study period were $57\pm11\%$ and $27.4\pm3.7\text{ }^\circ\text{C}$. As described in the section 2.3,
389 $f(RH)_{\text{water}}$ was calculated from the data from the two nephelometers. With the use of equations
390 1 and 2, we calculated LWC from the nephelometers for the whole measurement period. The
391 average value of $f(RH)_{\text{water}}$ was $2.19\pm1.75\text{ }\mu\text{g m}^{-3}$, which according to the dry mass
392 measurements, can contribute on average, up to 33% of the total submicron mass concentration.
393 We also sought to establish a link between $f(RH)$ and RH and taking into account all available
394 scattering data ($n=7044$) the following parameterization has been established:

$$395 \quad f(RH) = 1.067(\pm0.004) + 1.99(\pm1.05) \cdot 10^{-7} RH^{3.547(\pm0.035)} \quad (7)$$

396 Based on this, we reconstructed the time series of the hygroscopic growth factors, with a very good
397 correlation between calculated and measured values ($y=0.99x$, $R^2=0.85$) (also see Supplementary
398 Material). This parameterization does not appear to be influenced by changes in the chemical
399 composition. Uncertainties in the RH measurement by the probe are in the order of 5% while dry
400 and wet aerosol light scattering coefficients measurement uncertainty is in the order of 20%.

401

402 **3.2 Inorganic and organic water predictions**

403 **3.2.1 Inorganic aerosol water**

404 The thermodynamic model ISORROPIA-II (<http://isorropia.eas.gatech.edu>; Fountoukis and
405 Nenes, 2007) was used to predict the contribution of inorganic species to LWC. The water
406 attributed to the inorganic component of the aerosol has an average value of $1.77\pm1.45\text{ }\mu\text{g m}^{-3}$. The
407 lowest values are observed during August, probably because of the higher temperatures that
408 enhance evaporation of water from the aerosol. The timeseries for aerosol water associated both
409 with inorganic and organic aerosol components are shown in Figure 2, where it can be seen that
410 most of the time, the variability of the two water components follow each other closely, with water

411 concentrations associated with organics being about 1:10 (12±9%) of those associated with the
412 inorganic aerosol components.

413

414 **3.2.2 Organics: hygroscopicity and aerosol water**

415 The contribution of the organic submicron fraction of the aerosol to the particle water was
416 calculated from the combination of the CCN and chemical composition measurements, as
417 described in section 2.4. Assuming that the cumulative aerosol hygroscopicity can be represented
418 as the sum of contribution of the inorganic (expressed mostly by ammonium sulfate) and organic
419 fraction of the aerosol, the measured hygroscopicity can be calculated by the sum:

420
$$\kappa = \varepsilon_{inorg} \kappa_{inorg} + \varepsilon_{org} \kappa_{org} \quad (8)$$

421 where ε_j and κ_j are the volume fraction and hygroscopicity of the inorganic and organic species.
422 Once the aerosol species concentrations are determined, the corresponding volume fractions for
423 ammonium sulfate and organics are calculated, and a set of hygroscopicity parameter equations is
424 produced. As mentioned in the section 2.2, hygroscopicity parameters for 60, 80, 100 and 120 nm
425 particles are measured. In a former CCN study at the same site (Bougiatioti et al., 2011) it was
426 shown that from many different particle sizes, the characteristic hygroscopicity parameter κ^* of
427 the 100 nm particles was the closest one to the κ determined by PM₁ filter measurements. Therefore
428 we created two different sets of kappa equations along with the volume fractions to calculate the
429 total κ^* , one for the 100 and another one for the 120 nm. With the subsequent application of
430 multivariate regression analysis to the set of n=2429 and 1801 equations (for 100 and 120 nm
431 respectively), κ_{org} is determined to be 0.28±0.01 based on the κ_{100nm} and 0.24±0.01 based on the
432 κ_{120nm} . The average value of 0.26 is used in equation 5 to calculate the time series of W_{org} . The
433 average value W_{org} was thus found to be 0.56±0.37 $\mu\text{g m}^{-3}$, which constitutes on average ~27.5%
434 of the calculated $f(RH)_{water}$. The overall uncertainty of this calculation is estimated by Guo et
435 al. (2015) to be around 30%. That study for south eastern United States of America, found a higher
436 contribution of organic species (on average 35%) to the total water that can be explained by the
437 dominance of organics in the submicron range aerosol, with an average mass fraction of 67%.

438

439 **3.2.3. Aerosol water**

440 Aerosol water is the sum of $W_{org}+W_{inorg}$, determined as previously explained. This can be further
441 compared with the time series of the $f(RH)_{water}$ deduced from concurrent observations by the

442 two nephelometers (section 2.3), independent from the aerosol water calculated as here explained.
443 The particle water predicted from the sum of the organic and inorganic contributions to the water
444 agrees very well with the water measured by the nephelometers (Figure 3). More specifically, the
445 total predicted water is highly correlated and on average within 10% of the measured water, with
446 slope=0.92 and $R^2=0.8$ for the whole measurement period (n=5201 points).
447 The diurnal variability of the calculated water components, along with the total measured water,
448 ambient T and RH is shown in Figure 4. It must be noted at this point that the presented diurnal
449 variability corresponds to the entire period of the study and this pattern seems to be independent
450 of the geographical sector and/or source region, based on the backtrajectory analysis. The diurnal
451 variability of aerosols from different sources, further presented at Section 3.4, have been explicitly
452 studied and found not to differ significantly, therefore the total diurnal variability was selected as
453 being representative of the whole measurement period. Predicted and measured aerosol LWC
454 diurnal variabilities are in very good agreement. As expected, the highest LWC values are observed
455 during nighttime, when RH is also at its maximum, resulting in significant water uptake. W_{org}
456 shows a significant diurnal variability with morning and afternoon average mass concentrations
457 being 10-15 times lower than nighttime ones. Thus, during daytime W_{inorg} is the main component
458 of particle water as the average values for the predicted water ($W_{org}+W_{inorg}$) are very close to the
459 ones of the inorganic water alone. On the other hand, during nighttime, the two averages start to
460 diverge and this could be attributed to the higher contribution of organic water during nighttime,
461 when the photochemical activity and temperature are minimum and RH high.

462

463 **3.3 Aerosol pH**

464 The predicted pH for the aerosols collected at Finokalia during the studied period was highly acidic
465 with an average value of 1.25 ± 1.14 (median 1.51) and varying between -0.97 and 3.75. pH varied
466 by almost 1 unit throughout the day. This can be translated as an almost 10-fold increase of the
467 H^+_{air}/LWC ratio from early morning to mid-day and to a lesser extent during early night. This
468 significant variation in pH can be partially explained by the diurnal variation of H^+ and its increase
469 which coincides temporally with the decrease in pH (Figure 5) and by the reduction of aerosol
470 water (LWC) during daytime compared to the higher LWC during nighttime (Figure 4). This
471 implies the diurnal variability of pH is mostly driven by the reduction of aerosol water during
472 daytime compared to the higher aerosol water during nighttime.

473 When studying the diurnal variability of pH for the different sources/geographical sectors
474 (supplementary material) it occurs that pH differs depending on the source and origin of the air
475 masses. Air masses from the northwestern, northeastern Europe and Turkey, as well as from Greek
476 mainland, do not exhibit significant diurnal variability. When no distinction is made between
477 source regions, the pattern of the overall pH variability with a drop in pH values during midday as
478 presented in Fig. 5, is similar to the diurnal variability of pH for air masses influenced by mineral
479 dust (coming from the SW) and by biomass burning, but with pH values from biomass burning
480 being 1-1.5 units higher. Nevertheless, the mean pH values for each one of the source regions are
481 very close to the overall pH mean value when no distinction of origin is made.

482 Furthermore, accounting only for the water associated with the inorganic aerosol component,
483 particle water is underestimated by around 9%, thus resulting in a slightly lower pH (more acidic)
484 by 0.07-0.38 units of pH (Figure 6a). As seen in section 3.2, W_{org} is on average 27.5% of the total
485 water, as a result the pH increases by 0.14 units when the organic water is included (Figure 6a).
486 When the contribution of organic water is taken into account, the recalculation of pH gives an
487 average value of 1.38 ± 1.11 (median 1.65). The pH calculated by ISORROPIA-II correlates very
488 well with the pH corrected using equation 6 for inclusion of the organic water ($W_{org} + W_{inorg}$)
489 ($R^2=0.98$, Figure 6b). Subsequently, if organic mass and organic hygroscopicity data are not
490 available, ISORROPIA-II solely based on inorganic composition data, will provide an adequate
491 estimate of both H^+_{air} and W_{inorg} and thus of pH.

492

493 **3.4 Aerosol water and pH based on aerosol fraction and source region**

494 Apart from the time-resolved aerosol water and pH calculations for the submicron aerosol fraction,
495 aerosol water and pH were also calculated based on the daily PM_{10} filter chemical composition
496 analysis. It should be noted at this point that there is a strong link between aerosol pH and aerosol
497 size distribution due to the chemical composition changes in the aerosol size. For PM_1 which is in
498 equilibrium and chemical composition is determined by high time resolution measurements leads
499 to higher accuracy in the pH calculations. On the other hand, as PM_{10} particles are not in
500 equilibrium, the respective acidity results are subject to biases and are less quantitative than the
501 submicron results. For comparison purposes the corresponding PM_1 measurements, based on
502 ACSM and the respective PM_1 ionic concentrations for cations such as Na^+ , Ca^{2+} , Mg^{2+} , corresponding to
503 the fine fraction, have also been averaged to daily values. Characteristic source regions/sources

were subsequently selected based on back-trajectory analysis and chemical tracers. Furthermore, biomass burning events have been identified based on source apportionment of BC and Positive Matrix Factorization (PMF) analysis of the organic mass spectra obtained from the ACSM as detailed in Bougiatioti et al. (2014). Dust events were identified by backtrajectory analysis of the air masses, originating from Northwestern Africa and confirmed as by containing large amounts of particulate matter ($45\text{--}55 \mu\text{g m}^{-3}$ in PM_{10} mass) and high concentrations of crustal ions, such as Ca^{2+} (median concentration during dust events of $1.8 \mu\text{g m}^{-3}$ versus $0.6 \mu\text{g m}^{-3}$ for the rest of the days) . The main measured and calculated parameters are presented in Table 1.

It can be seen that, in general, for anthropogenic-laden air masses (e.g. from Istanbul, Black Sea and Continental Europe) aerosol mass resides mainly (60-70%) in the submicron aerosol and thus the submicron fraction seems also to drive the pH of PM_{10} , while most of the aerosol water (~70%) is present in the coarse fraction. Biomass burning exhibits the highest values of pH in the submicron fraction and the lowest values in total water mass concentration. Interestingly enough, the value of 2.77 for biomass burning pH is well above the value of 2, which favors the partitioning of nitrate to the aerosol phase (e.g., Meskhidze et al., 2003) The correlation observed during fire events between biomass burning organic aerosol and particulate nitrates (e.g. Bougiatioti et al., 2014) may be explained by these higher pH levels, rather than just high levels of nitric acid and/or ammonia. As found in the literature, higher pH levels of biomass burning aerosol ~~can also could possibly be attributed to associated with~~ higher concentrations of non-sea salt potassium, which as an ionic species influences pH (Zhang et al. 2015), rendering aerosol ~~more alkaline less acidic~~. Based on the calculated ratios for pH and particle water, it can be derived that the ions that set the bulk pH is mostly driven by the fine mode; the LWC however is associated mostly with the supermicron aerosol mass. Hygroscopic sea salt components are also found in the coarse mode, which can justify the larger contribution of PM_{10} total water, while the submicron fraction may be composed mostly of less hygroscopic, organic components (Bougiatioti et al., 2015). Even though strong dust events were lacking during the study period, numerous weaker events were captured. From these events it occurs that aerosol mass, total water and pH are mostly driven by the coarse aerosol fraction. This is consistent with the findings of Koulouri et al. (2008) that most (86%) of the mass of crustal components were found in coarse particles. In terms of mass concentration, the two natural sources, namely air masses of marine and dust origin, contain the largest amounts of total submicron water. Even though total water exhibits the highest mass concentrations for the

535 specific sources, the relative contribution of organic water to the submicron fraction is the lowest
536 (16% for dust and 17% for marine, based on the median values). For the two natural sources, the
537 ratio between submicron pH and calculated pH for the PM₁₀ fraction is the lowest observed (Table
538 1), namely 30±17% (median 25%) and 6±19% (median 5%).

539

540 **3.5 Atmospheric implications**

541 The pH values for submicron and PM₁₀ fractions is also expected to affect many processes, such
542 as the solubility and therefore the bioavailability of nutrients and especially phosphorus (P) and
543 iron (Fe). This is of crucial importance for seas such as the eastern Mediterranean for which
544 primary productivity is P limited (Krom et al., 1991). One of the striking results of the aerosol pH
545 calculations (presented in Table 1) is that with the exception of biomass burning, pH of all
546 submicronic aerosols including those originating from desert dust is highly acidic with values
547 typically below 2. Although the nutrient flux from the fine mode is certainly smaller than in the
548 coarse mode, it can be transported much further away from source regions before deposition, and
549 be considerably more acidified (hence bioavailable). Based on published literature (Nenes et al.,
550 2011; Meskhidze et al., 2003) under acidic conditions similar to the derived pH aerosol values, the
551 acid-mobilized dissolution of such nutrients is expected to be of great importance.

552 Markaki et al. (2003), by analyzing PM₁₀ aerosols collected in Greece (Finokalia) and Turkey
553 (Erdemli) for dissolved inorganic (DIP) and Total (TP) phosphorus levels have shown that
554 although the SW sector, corresponding to the Sahara, presented TIP levels by a factor of two higher
555 than the European (NE or NW) sectors, the lowest values for the DIP/TIP ratio are associated with
556 the SE and SW sectors, and the highest with the N sectors (difference of almost a factor of 2). The
557 explanation for that behavior is given by the ratio of pH in PM₁ and PM₁₀ aerosols that is presented
558 in Table 1. In aerosols from the NW sector only a very small difference in pH between the two
559 fractions is observed, while in desert aerosols the large amount of dust present in the coarse mode
560 highly influences pH of PM₁₀ leading to a significant decrease of acidity and thus P solubility.
561 However as dust events can transport large amounts of P (up to a factor of three higher than in air
562 masses coming from Europe), any future change in PM₁/PM₁₀ ratio caused by dust events will
563 significantly influence P availability and deposition to the eastern Mediterranean sea and thus to
564 its productivity.

565

566 **Conclusion**

567 Using the aerosol chemical composition measurements by ACSM, thermodynamic models, such
568 as ISORROPIA-II, and CCN measurements we calculated the particle water associated with both
569 inorganics (W_{inorg}) and organics (W_{org}) aerosol components. The sum of these two ($W_{inorg}+W_{org}$)
570 equal to the total particle water is then compared to the LWC determined by the two nephelometers
571 operating in dry and wet mode, respectively. Predicted aerosol water was compared to LWC
572 determined from ambient versus dry light scattering coefficients. At Finokalia the sum of W_{inorg}
573 and W_{org} was highly correlated and in close agreement with the measured LWC (on average within
574 10%), with slope=0.92 and $R^2=0.8$ for the whole measurement period (n=5201 points). As
575 expected, the highest fine aerosol water values are observed during nighttime, when RH is also at
576 its maximum, resulting in significant water uptake. W_{org} shows a significant diurnal variability
577 with morning and afternoon average mass concentrations being 10-15 times lower than nighttime
578 concentrations. Thus, during daytime W_{inorg} is the main form of particle water as the average values
579 for the predicted water ($W_{org}+W_{inorg}$) are very close to the ones of the inorganic water alone. On
580 the other hand, the contribution of organic water to the total aerosol water increases becoming
581 significant during nighttime, when the photochemical activity and temperature are minimum. The
582 average concentration of total aerosol water was found to be $2.19\pm1.75 \mu\text{g m}^{-3}$, which according
583 to the dry mass measurements, can contribute on average up to 33% of the total submicron mass
584 concentration. The average aerosol water associated with organics, W_{org} , was found to be
585 $0.56\pm0.37 \mu\text{g m}^{-3}$, which constitutes about 27.5% of the total calculated water. The overall
586 uncertainty of this calculation is estimated to be around 30%.

587 Based on aerosol water, particle pH is also calculated, a parameter which is very important for the
588 atmospheric implications of aerosols but is difficult to measure directly. In the eastern
589 Mediterranean during the studied period, aerosol pH varied from 0.5 to 2.8 indicating that the
590 aerosol was highly acidic throughout the period. Biomass burning aerosol presented the highest
591 values of pH in the submicron fraction and the lowest values in total water mass concentration.
592 Interestingly enough, the value of 2.8 for biomass burning pH is well above the value of 2, which
593 is a lower limit for the occurrence of nitrate's condensation. The correlation, which has been
594 observed during fire events between biomass burning organic aerosol and particulate nitrates, may
595 be explained by these pH levels, which favor nitrate condensation. It can be seen that, in general,
596 for anthropogenic-laden air masses (e.g. from Istanbul, Black Sea and Continental Europe) aerosol

597 mass resides mainly in the submicron aerosol (60-70%) and thus the submicron fraction seems
598 also to drive the pH of PM₁₀, while most of the aerosol water (~70%) is present in the coarse
599 fraction. pH is driven by the fine mode while on the contrary, the grand majority of the aerosol
600 water is present in the coarse mode. This may be due to the important contributions of the
601 hygroscopic sea salt components in the coarse mode and of the less hygroscopic organics in the
602 fine mode.

603 In terms of mass concentration, the air masses affected by the two natural sources, namely of
604 marine and dust origin, contain the largest amounts of total submicron water. Even though total
605 water exhibits the highest mass concentrations for the specific sources, the relative contribution of
606 organic water to the submicron fraction is the lowest (~19% for dust and ~15.5% for marine). For
607 these two natural sources, the ratio between submicron pH and calculated pH for the PM₁₀ fraction
608 is the lowest observed, 30±17% (median 25%) and 6±19% (median 5%).

609 The low pH values observed during the studied period in the submicron mode and independently
610 of air masses origin could have significant implications for nutrient availability and especially for
611 P solubility which is the nutrient limiting sea water productivity of the eastern Mediterranean.

612

613 **Acknowledgments.** This research has been co-financed by the European Union (European Social
614 Fund – ESF) and Greek national funds through the Operational Program "Education and Lifelong
615 Learning" of the National Strategic Reference Framework (NSRF) - Research Funding Program
616 ARISTEIA I - PANOPLY. The authors gratefully acknowledge the NOAA Air Resources
617 Laboratory (ARL) for the provision of the HYSPLIT transport and dispersion model and READY
618 website (<http://www.ready.noaa.gov>) used in this publication.

619

620

621

622

623

624 **References**

625 APHA, AWWA, WEF, (2000) Standard Methods for the Examination of Water and Wastewater,
626 20th ed. American Public Health Association, Washington DC.

627 Bougiatioti, A., Zarmpas, P., Koulouri, E., Antoniou, M., Theodosi, C., Kouvarakis G., Saarikoski,
628 S., Mäkelä, T., Hillamo, R., and Mihalopoulos, N.: Organic, elemental and water-soluble organic
629 carbon in size segregated aerosols, in the marine boundary layer of the Eastern Mediterranean,
630 Atmos. Environ., 64, 251-262, 2013.

631 Bougiatioti A., Stavroulas, I., Kostenidou, E., Zarmpas, P., Theodosi, C., Kouvarakis, G.,
632 Canonaco, F., Prévôt, A.S.H., Nenes, A., Pandis, S.N., and Mihalopoulos, N.: Processing of
633 biomass-burning aerosol in the easter Mediterranean during summertime, Atmos. Chem. Phys.,
634 14, 4793-4807, doi:10.5194/acp-14-4793-2014, 2014.

635 Bougiatioti, A., Bezantakos, S., Stavroulas, I., Kalivitis, N., Kokkalis, P., Biskos, G.,
636 Mihalopoulos, N., Papayannis, A., and Nenes, A.: Influence of biomass burning on CCN number
637 and hygroscopicity during summertime in the eastern Mediterranean, Atmos. Chem. Phys.
638 Discuss., 15, 21539-21582, doi:10.5194/acpd-15-21539-2015, 2015.

639 Carlton, A. G. and Turpin, B. J.: Particle partitioning potential of organic compounds is highest in
640 the Eastern US and driven by anthropogenic water, Atmos. Chem. Phys., 13, 10203–10214,
641 doi:10.5194/acp-13-10203-2013, 2013.

642 Cerully, K. M., Bougiatioti, A., Hite Jr., J. R., Guo, H., Xu, L., Ng, N. L., Weber, R., and Nenes,
643 A.: On the link between hygroscopicity, volatility, and oxidation state of ambient and water-
644 soluble aerosol in the Southeastern United States, Atmos. Chem. Phys. Discuss., 14, 30835-
645 30877, doi:10.5194/acpd-14-30835-2014, 2014.

646 Eddingsaas, N. C., VanderVelde, D. G., and Wennberg, P. O.: Kinetics and Products of the Acid-
647 Catalyzed Ring-Opening of Atmospherically Relevant Butyl Epoxy Alcohols, J. Phys. Chem.
648 A, 114, 8106–8113, doi:10.1021/Jp103907c, 2010.

649 Fountoukis, C., and Nenes, A.: ISORROPIA II: a computationally efficient thermodynamic
650 equilibrium model for K^+ - Ca^{2+} - Mg^{2+} - NH_4^+ - Na^+ - SO_4^{2-} - NO_3^- - Cl^- - H_2O aerosols, Atmospheric
651 Chemistry and Physics, 7, 4639-4659, 2007.

652 Fountoukis, C., Nenes, A., Sullivan, A., Weber, R., Van Reken, T., Fischer, M., Matias, E., Moya,
653 M., Farmer, D., and Cohen, R. C.: Thermodynamic characterization of Mexico City aerosol
654 during MILAGRO 2006, Atmospheric Chemistry and Physics, 9, 2141-2156, 2009.

655 Guo, H., Xu, L., Bougiatioti, A., Cerully, K.M., Capps, S.L., Hite, J.R., Carlton, A.G., Lee, S.-H.,
656 Bergin, M.H., Ng, N.L., Nenes, A., and Weber, R.J.: Particle water and pH in the southeastern
657 United States, *Atmospheric Chemistry and Physics*, 15, 5211-5228, doi:10.5194/acp-15-5211-
658 2015, 2015.

659 Hennigan, C. J., Izumi, J., Sullivan, A. P., Weber, R. J., and Nenes, A.: A critical evaluation of
660 proxy methods used to estimate the acidity of atmospheric particles, *Atmos. Chem. Phys.*, 15,
661 2775– 2790, doi:10.5194/acp-15-2775-2015, 2015.

662 Jickells, T.D., Z. S. An, K. K. Andersen, A. R. Baker, G. Bergametti, N. Brooks, J. J. Cao, P. W.
663 Boyd, R. A. Duce, K. A. Hunter, et al., Global iron connections between desert dust, ocean
664 biogeochemistry, and climate. *Science* 308:67–71, 2005.

665 Keene, W. C., A. A. P. Pszenny, J. R. Maben, and R. Sander: Variation of marine aerosol acidity
666 with particle size, *Geophys. Res. Lett.*, 29(7), doi:10.1029/2001GL013881, 2002.

667 Keene, W.C., Pszenny, A.A.P., Maben, J.R., Stevenson, E., Wall, A.: Closure evaluation of size-
668 resolved aerosol pH in the New England coastal atmosphere during summer, *J. Geophys. Res.*,
669 109, D23307, doi:10.1029/2004JD004801, 2004.

670 Khlystov, A., Stanier, C.O., Takahama, S. and Pandis, S.N.: Water content of ambient aerosol
671 during the Pittsburgh Air Quality Study, *J. Geophys. Res. Atmospheres*, Vol 110, Issue D7,
672 doi:10.1029/2004JD004651, 2005.

673 Kim, J., Yoon, S.-C., Jefferson, A., and Kim, S.-W.: Aerosol hygroscopic properties during Asian
674 dust, pollution, and biomass burning episodes at Gosan, Korea in April 2001, *Atmospheric 635
675 Environment*, 40, 1550-1560, 10.1016/j.atmosenv.2005.10.044, 2006.

676 Koulouri, E., Saarikoski, S., Theodosi, C., Markaki, Z., Gerasopoulos, E., Kouvarakis, G., Mäkelä,
677 T., Hillamo, R., and Mihalopoulos, N.: Chemical composition and sources of fine and coarse
678 aerosol particles in the Eastern Mediterranean, *Atmos. Environ.*, 42, 6542-9550, 2008.

679 Kouvarakis, G. Mihalopoulos, N., Tselepidis, T., Stavrakakis, S.: On the importance of
680 atmospheric nitrogen inputs on the productivity of Easter Mediterranean, *Global Biochem.
681 Cycles*, 15, 805-818, 2001.

682 Kreidenweis, S. M., Petters, M. D., and DeMott, P. J.: Singleparameter estimates of aerosol water
683 content, *Environ. Res. Lett.*, 3, 035002, doi:10.1088/1748-9326/3/3/035002, 2008.

684 Krishnamurthy, A., Moore, J.K., Mahowald, N., Luo, C., and Zender, C.S.: Impacts of atmospheric
685 nutrient inputs on marine biogeochemistry, *J. Geophys. Res.*, 115, G01006,
686 doi:10.1029/2009JG001115, 2010.

687 Krom, M.D., Kress, N., Brenner, S., and Gordon, L.I.: Phosphorus limitation of primary
688 productivity in the eastern Mediterranean Sea, *Limnol. Oceanogr.*, 36 (3), 424-432, 1991.

689 Lee, T., Sullivan, A. P., Mack, L., Jimenez, J. L., Kreidenweis, S. M., Onasch, T. B., Worsnop, D.
690 R., Malm, W., Wold, C. E., Hao, W. M., and Collett, J. L.: Variation of chemical smoke marker
691 emissions during flaming vs. smoldering phases of laboratory open burning of wildland fuels,
692 *Aerosol Sci. Technol.*, 44, 1–5, doi:10.1080/02786826.2010.499884, 2010.

693 Liao, H. and Seinfeld, J. H.: Global impacts of gas-phase chemistry aerosol interactions on direct
694 radiative forcing by anthropogenic aerosols and ozone, *J. Geophys. Res.-Atmos.*, 110, D18208,
695 doi:10.1029/2005jd005907, 2005.

696 Magi, B. I.: Effects of humidity on aerosols in southern Africa during the biomass burning season,
697 *Journal of Geophysical Research*, 108, doi:10.1029/2002jd002144, 2003.

698 Mahowald, N., Jickells, T.D., Baker, A.R., Artaxo, P., Benitez-Nelson, C.R., Bergametti, J., Bond,
699 T.C., Chen, Y., Cohen, D.D., Herut, B., Kubilay, N., Losno, R., Luo, C., Maenhaut, W.,
700 McGee, K.A., Okin, G.S., Siefert, R.L., and Tsukuda, S.: Global distribution of atmospheric
701 phosphorus sources, concentrations and deposition rates, and anthropogenic impacts, *Global
702 Biogeochem. Cycles*, 22, GB4026, doi:10.1029/2008GB003240, 2008.

703 Mahowald, N. M., Engelstaedter, S., Luo, C., Sealy, A., Artaxo, P., Benitez-Nelson, C., Bonnet,
704 S., Chen, Y., Chuang, P.Y., Cohen, D.D., Dulac, F., Herut, B., Johansen, A.M., Kubilay, N.,
705 Losno, R., Maenhaut, W., Paytan, A., Prospero, J.M., Shank, L.M., and Siefert, R.L.:
706 Atmospheric iron deposition: Global distribution, variability, and human perturbations, *Annu.
707 Rev. Mater. Sci.*, 1, 245–278, doi:10.1146/annurev.marine.010908.163727, 2009.

708 Meskhidze, N., Chameides, W.L., Nenes, A., and Chen, G.: Iron mobilization in mineral dust: Can
709 anthropogenic SO₂ emissions affect ocean productivity?, *Geophys. Res. Lett.*, 30 (21),
710 doi:10.1029/2003GL018035, 2003.

711 Meskhidze, N., Chameides, W. and Nenes, A. (2005) Dust and Pollution: A Recipe for Enhanced
712 Ocean Fertilization? *J. Geophys. Res.*, 110, D03301, doi:10.1029/2004JD005082

713 Mihalopoulos, N., Stephanou, E., Kanakidou, M., Pilitsidis, S., and Bousquet, P.: Tropospheric
714 aerosol ionic composition above the eastern Mediterranean area, *Tellus B*, **49**, 314–326,
715 1997. Moore, R.H., and Nenes, A.: Scanning Flow CCN Analysis-A method for fast
716 measurements of CCN spectra, *Aerosol Sci. Technol.*, 43:12, 1992-1207, 2009.

717 Myriokefalitakis, S., Tsigaridis, K., Mihalopoulos, N., Sciare, J., Nenes, A., Kawamura, K.,
718 Segers, A., and Kanakidou, M.: In-cloud oxalate formation in the global troposphere: a 3-D
719 modeling study, *Atmos. Chem. Phys.*, 11, 5761–5782, doi:10.5194/acp-11-5761-2011, 2011.

720 Myriokefalitakis, S., Daskalakis, N., Mihalopoulos, N., Baker, A. R., Nenes, A., and
721 Kanakidou, M.: Changes in dissolved iron deposition to the oceans driven by human activity: a
722 3-D global modelling study, *Biogeosciences*, 12, 3973-3992, doi:10.5194/bg-12-3973-2015,
723 2015.

724 Nenes, A., Krom, M. D., Mihalopoulos, N., Van Cappellen, P., Shi, Z., Bougiatioti, A., Zarmpas,
725 P., and Herut, B.: Atmospheric acidification of mineral aerosols: a source of bioavailable
726 phosphorus for the oceans, *Atmos. Chem. Phys.*, 11, 6265–6272, doi:10.5194/acp-11-6265-
727 2011, 2011.

728 Ng, N.L., Herndon, S.C., Trimborn, A., Canagaratna, M.R., Croteau, P.L., Onasch, T.B., Sueper,
729 D., Worsnop, D.R., Zhang, Q., Sun, Y.L., and Jayne, J.T.: An Aerosol Chemical Speciation
730 Monitor (ACSM) for routine monitoring of the composition and mass concentration of ambient
731 aerosol., *Aerosol Sci. Technol.*, **45** (7), 780-794, 2011.

732 Nguyen, T.K.V., Petters, M.D., Suda, S.R., Guo, H., Weber, R.J., and Carlton, A.G.: Trends in
733 particle-phase liquid water during the Southern Oxidant and Aerosol Study, *Atmos. Chem.*
734 *Phys.*, 14, 10911-10930, doi:10.5194/acp-14-10911-2014, 2014.

735 Nowak, J. B., Huey, L. G., Russell, A. G., Tian, D., Neuman, J. A., Orsini, D., Sjostedt, S. J.,
736 Sullivan, A.P., Tanner, D. J., Weber, R. J., Nenes, A., Edgerton, E., and Fehsenfeld, F. C.:
737 Analysis of urban gas phase ammonia measurements from the 2002 Atlanta Aerosol Nucleation
738 and Real-Time Characterization Experiment (ANARChE), *Journal of Geophysical Research*,
739 111, 10.1029/2006jd007113, 2006.

740 Petters, M.D., and Kreidenweis, S.M.: A single parameter representation of hygroscopic growth
741 and cloud condensation nucleus activity, *Atmos. Chem. Phys.*, 7, 1961-1971, doi: 10.5194/acp-
742 8-6273-2008, 2007.

743 Pilinis, C., Pandis, S. N., and Seinfeld, J. H.: Sensitivity of Direct Climate Forcing by Atmospheric
744 Aerosols to Aerosol-Size and Composition, *J. Geophys. Res.-Atmos.*, 100, 18739–18754,
745 doi:10.1029/95jd02119, 1995.

746 Pöschl, U., and Shiraiwa, M.: Multiphase chemistry at the atmosphere-biosphere interface
747 influencing climate and public health in the Anthropocene, *Chem. Rev.*, 115, 4440-4475,
748 doi:10.2021/cr500487s, 2015

749 Roberts, G.C., and Nenes, A.: A continuous-flow streamwise thermal-gradient CCN chamber for
750 atmospheric measurements, *Aerosol Sci. Technol.*, 39, 206-221,
751 dpo:10.1080/027868290913988, 2005.

752 Sheridan, P. J.: Spatial variability of submicrometer aerosol radiative properties over the Indian
753 Ocean during INDOEX, *Journal of Geophysical Research*, 107, 10.1029/2000jd000166, 2002.

754 Shi, Z., Krom, M.D., Jickells T.D., Bonneville, S., Carslaw, K.S., Mihalopoulos, N., Baker, A.R.,
755 Benning, L.G.: Impacts on iron solubility in the mineral dust by processes in the source region
756 and the atmosphere: A review, *Aeol. Res.* 5, 21–42, doi:/10.1016/j.aeolia.2012.03.001, 2012.

757 Solmon, F., Chuang, P.Y., Meskhidze, N., and Chen, Y.: Acidic processing of mineral dust iron
758 by anthropogenic compounds over the north Pacific Ocean, *J. Geophys. Res., Atmospheres*,
759 114 (D2), doi:10.1029/2008JD010417, 2009.

760 Spindler, G., Hesper, J., Brüggemann, E., Dubois R., Müller, Th., and Herrmann, H.: Wet annular
761 denuder measurements of nitrous acid: laboratory study of the artefact reaction of NO₂ with
762 S(IV) in aqueous solution and comparison with field measurements, *Atmos. Environ.*, 37, 2643-
763 2662, 2003.

764 A. F. Stein, R. R. Draxler, G. D. Rolph, B. J. B. Stunder, M. D. Cohen, and F. Ngan, 2015: NOAA's
765 HYSPLIT Atmospheric Transport and Dispersion Modeling System. *Bull. Amer. Meteor.*
766 *Soc.*, **96**, 2059–2077, doi: <http://dx.doi.org/10.1175/BAMS-D-14-00110.1>, 2015.

767 Stookey, L. C.: Ferrozine - a new spectrophotometric reagent for iron. *Analytical Chemistry* 42,
768 779–781, 1970.

769 Stumm, W. and Morgan, J. J.: *Aquatic Chemistry*, Wiley- Interscience, New York, 1996.

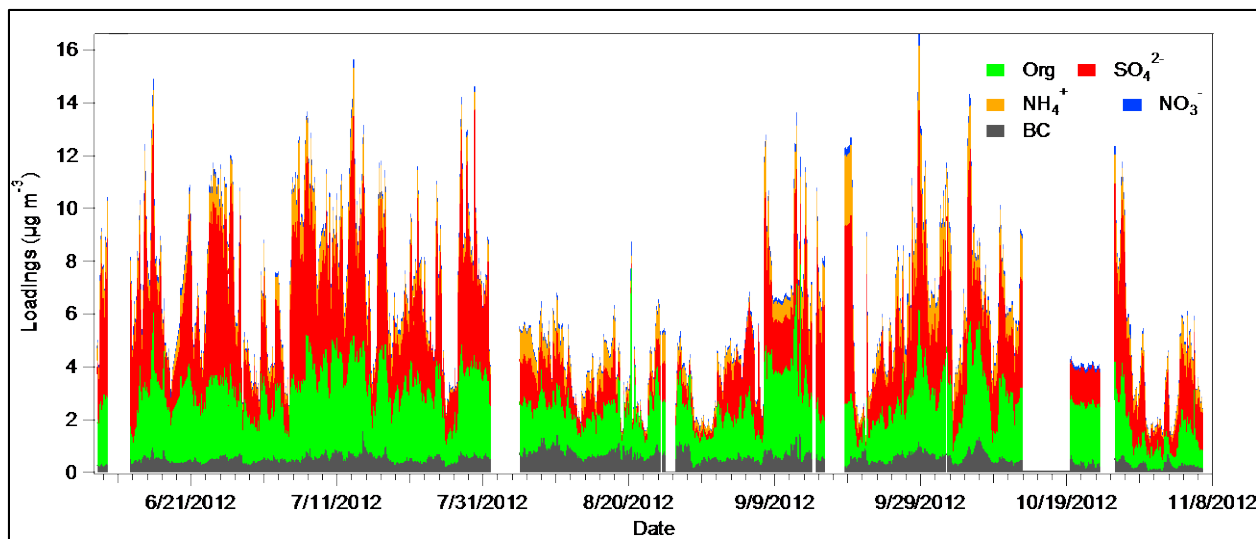
770 Surratt, J. D., Lewandowski, M., Offenberg, J. H., Jaoui, M., Kleindienst, T. E., Edney, E. O., and
771 Seinfeld, J. H.: Effect of acidity on secondary organic aerosol formation from isoprene, *Environ.*
772 *Sci. Technol.*, 41, 5363–5369, doi:10.1021/es0704176, 2007.

773 Surratt, J. D., Chan, A. W., Eddingsaas, N. C., Chan, M., Loza, C. L., Kwan, A. J., Hersey, S. P.,
774 Flagan, R. C., Wennberg, P. O., and Seinfeld, J. H.: Reactive intermediates revealed in secondary
775 organic aerosol formation from isoprene, *P. Natl. Acad. Sci. USA*, 107, 6640–6645,
776 doi:10.1073/pnas.0911114107, 2010.

777 Weber, R.J., Guo, H., Russel, A.G., and Nenes, A.: High aerosol acidity despite declining
778 atmospheric sulfate concentrations over the past 15 years, *Nat. Geosci.*, L3,
779 doi:10.1038/ngeo2665, 2016.

780 Wyers, G.P., Otjes, R.P., Slanina, J.: A continuous-flow denuder for the measurement of ambient
781 concentrations and surface-exchange fluxes of ammonia, *Atmos. Environ.*, 27, 2085–2090,
782 1993.

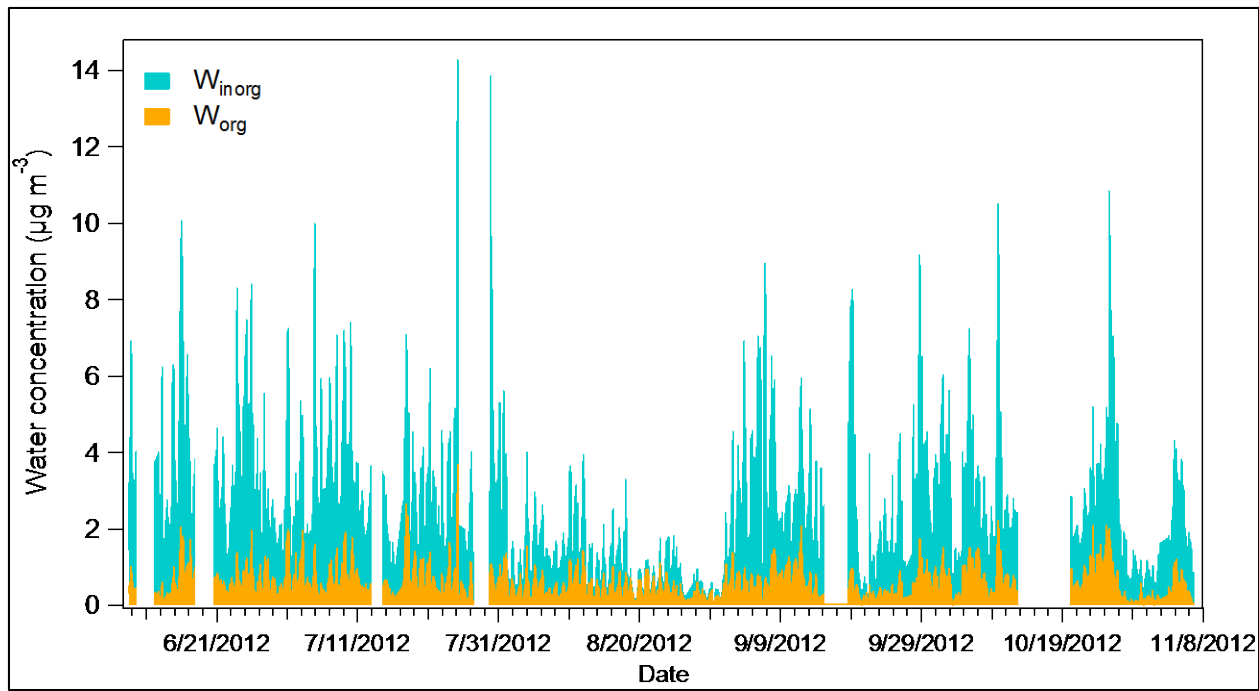
783 Zhang, Z., Gao, J., Engling, G., Tao, J., Chai, F., Zhang, L., Zhang, R., Sang, X., Chan, C., Lin,
784 Z., and Cao, J.: Characteristics and applications of size-segregated biomass burning tracers in
785 China's Pearl River Delta region, *Atmos. Environ.*, 102, 290-301, 2015.



786

787 **Figure 1:** Time series of the main submicron aerosol components at Finokalia, Crete, during the
788 measurement period in 2012.

789

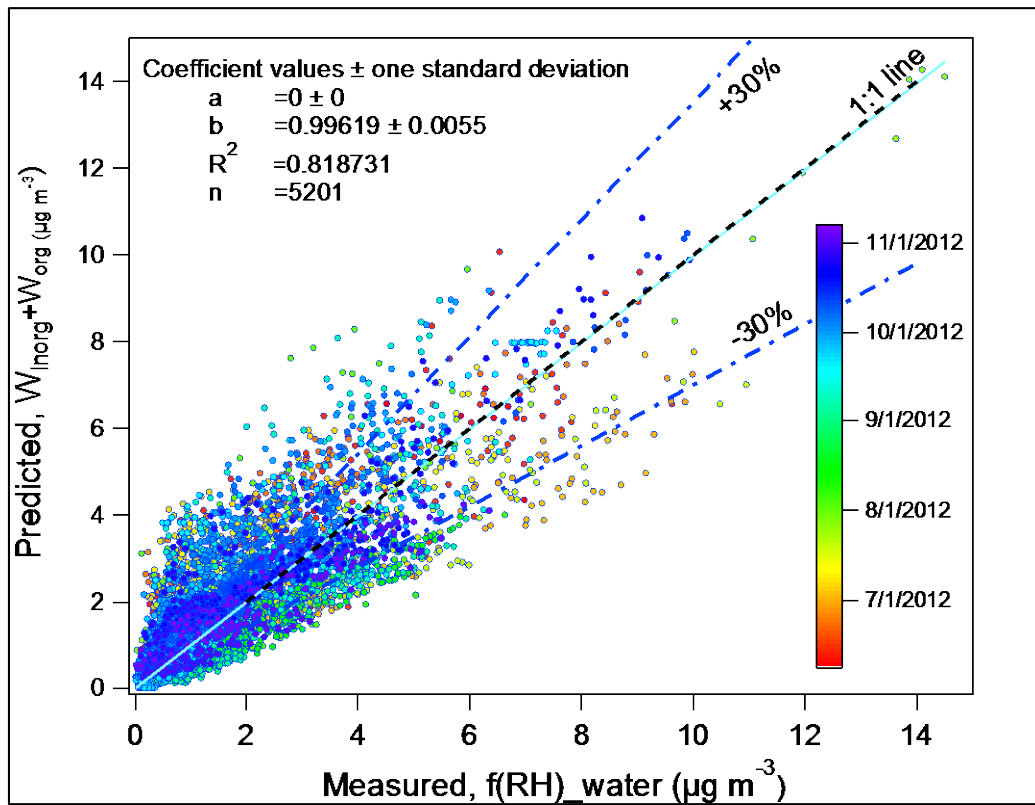


790

791 **Figure 2:** Time series of the two calculated aerosol water components, the water associated with
792 the inorganic (W_{inorg}) and the organic (W_{org}) aerosol components.

793

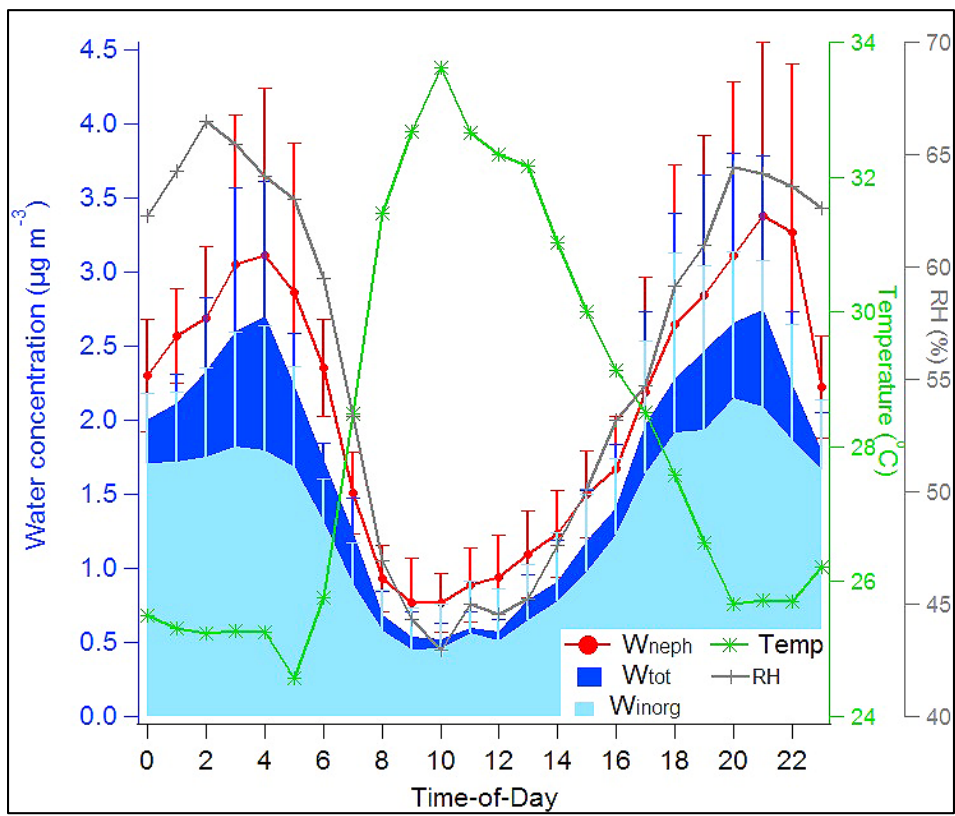
794



795

796 **Figure 3:** Correlation between calculated and measured LWC of aerosol.

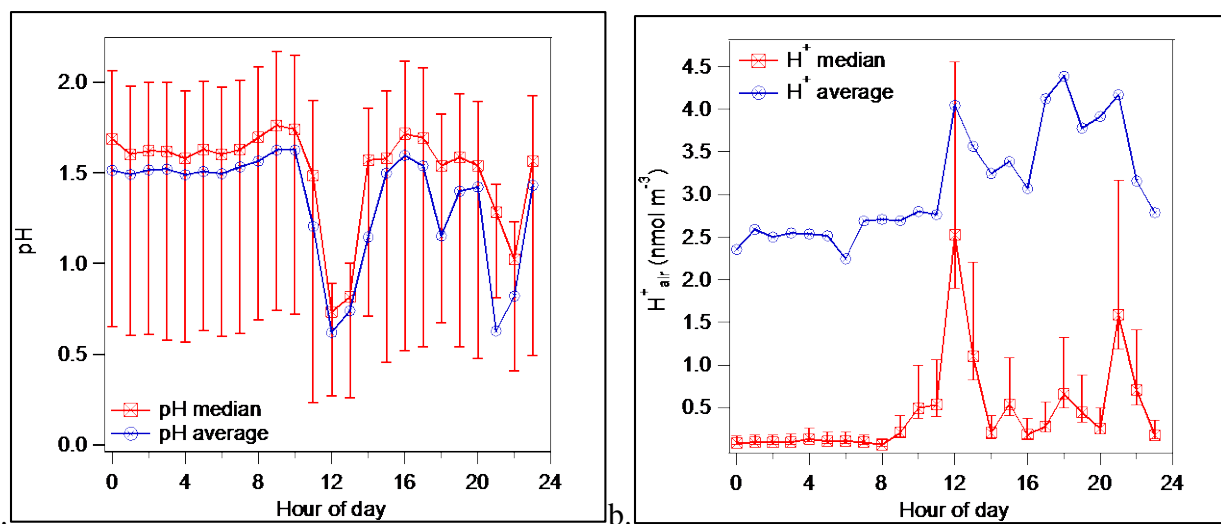
797



799
800 **Figure 4:** Diurnal profiles of predicted and measured water, along with measured RH and T.
801 Average hourly averages and standard deviations plotted as error bars in local hour are shown.
802

803

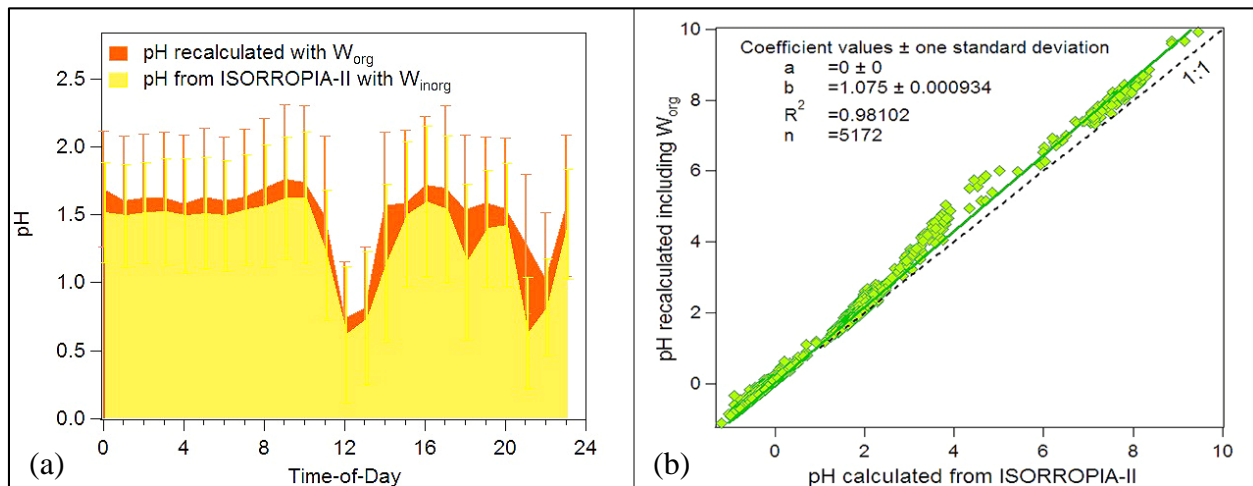
804



805 **Figure 5:** Diurnal profile of pH (a) and H^+ (b) calculated based on total predicted water and
 806 hydronium concentrations predicted by ISORROPIA-II. Average and median (with 25%, 75%
 807 quantiles) values are provided.

808

809
810



811 **Figure 6:** a) Diurnal variability of pH based on total predicted water (orange using both W_{org} and
812 W_{inorg}) and only the inorganic water (yellow using only W_{inorg}), respectively. Average hourly
813 values and standard deviation in the form of error bars are provided, b) Comparison between the
814 pH predicted by ISORROPIA-II based on inorganic aerosol composition and that recalculated
815 including also the organic component.

816
817
818
819
820
821
822
823
824
825
826
827
828
829

830 **Table 1:** Average values of water content (total and organic) and pH with standard deviation and
 831 median values in parenthesis.

832

Source / region	PM ₁			PM ₁ /PM ₁₀		
	water _{tot} ($\mu\text{g m}^{-3}$)	water _{org} ($\mu\text{g m}^{-3}$)	pH	mass	water _{tot}	pH
Biomass	1.33 \pm 1.22	0.37 \pm 0.33	2.77 \pm 0.88	0.48 \pm 0.16	0.08 \pm 0.09	0.89 \pm 0.2
Burning (n=7)	(1.56)	(0.39)	(2.67)	(0.47)	(0.05)	(0.93)
Istanbul & Black Sea (n=7)	1.72 \pm 0.54	0.81 \pm 0.34	1.92 \pm 0.24	0.72 \pm 0.09	0.33 \pm 0.21	0.94 \pm 0.67
Continental Europe (n=9)	1.52 \pm 0.64	0.48 \pm 0.34	1.30 \pm 0.19	0.60 \pm 0.18	0.31 \pm 0.17	0.58 \pm 0.47
Dust (n=7)	2.48 \pm 0.54	0.48 \pm 0.22	1.48 \pm 0.44	0.34 \pm 0.08	0.39 \pm 0.08	0.30 \pm 0.17
Marine (n=7)	2.38 \pm 1.24	0.37 \pm 0.17	0.44 \pm 0.67	0.58 \pm 0.27	0.83 \pm 0.6	0.06 \pm 0.19
	(1.91)	(0.34)	(0.43)	(0.57)	(0.70)	(0.05)

833